COMMUNICATION

High Performance Polyanthraquinone/$Ni(OH)_2$ Aqueous Batteries Based on Hydroxyl and Potassium Insertion/Extraction Reactions

Chang Liu,[a] Ting Ma,[a] Kexin Xia,[a] Xuesen Hou,[a] Qingshun Nian[a], Yichao Cai[a] and Jing Liang*[ab]
a. Key Laboratory of Advanced Energy Materials Chemistry, Ministry of Education, College of Chemistry, Nankai University, Tianjin 300071, PR China
b. Renewable Energy Conversion and Storage Center, Nankai University, Tianjin 300071, PR China
*Corresponding Author: liangjing@nankai.edu.cn

Experimental Details

Materials and Equipment

N,N-Dimethylformamide (DMF) was anhydrous grade and dried over molecular sieves prior to use. All other chemicals were reagent grade and used as received. ^{1}H NMR and ^{13}C NMR spectra were recorded using AVANCE III 400MHz (Bruker) NMR spectrometers. Chemical shifts were referenced to residual protons or carbons in deuterated solvents. Infrared (IR) spectra were recorded for solid samples on a Bruker Tensor II sample compartment RT-DLaTGS spectrometer using attenuated total reflectance (ATR) technique. Matrix-assisted laser desorption/ionization time-of-flight mass spectroscopy (MALDI-TOF-MS) was recorded on a Bruker AutoflexIII LRF200-CID spectrometer. Scanning electron microscopy (SEM) was performed on a SEM, JEOL JSM78500F microscope. Transmission electron microscope (TEM) was performed on a Talos F200X G2, AEMC microscope (Bruker Tensor II sample compartment RT-DLaTGS). Thermogravimetry (TG) was measured on a thermogravimetric analyzer (NETZSCH, STA 449F3). Cyclic voltammograms were obtained on a Parstat 2263 electrochemical workstation (Princeton Applied Research and AMETEK Company). The first scan of P14AQ was in a reductive direction and the one of Co-$Ni(OH)_2$ was in a oxidative direction. The discharge/charge tests were conducted on a LAND-CT2001A battery testing instrument.

Synthesis of Poly(1,4-anthraquinone) (P14AQ)

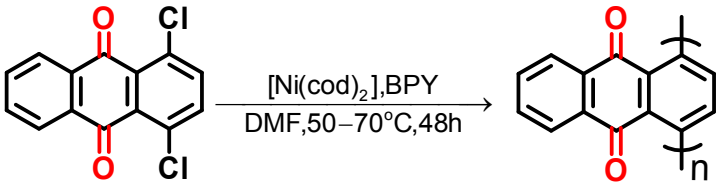

1,4-DCAQ P14AQ

Bis(1,5-cyclooctadiene)nickel(0) ($Ni(COD)_2$, 2.2 g, 8 mmol), 2,2'-bipyridine (1.25 g, 8 mmol), and 1,5-cyclooctadiene (COD, 0.74 mL, 6 mmol) were first dissolved in 60 mL dimethyl formamide (DMF)[1]. 1,4-dichloroanthraquinone (1.4-DCAQ, 1.662 g, 0.003 mol) was then dissolved in 40 mL DMF and added into the above solution. The mixture reacted at 50-70 °C for 48 h under argon flow. After cooling to room temperature, the mixture was poured into 100 mL diluted hydrochloric acid (0.5 M), immediately generating yellow precipitate. The product was filtered and washed several times successively with DMF, diluted hydrochloric acid, warm deionized water and methanol, then dried at 80 °C in vacuum for 12 h. To purify P14AQ, as-prepared product was dissolved in dichloromethane and recrystallized by adding methanol. The final yield of P14AQ under 50°C, 60°C and 70°C is around 60%, 80% and 85%, respectively. The product was characterized by NMR, FTIR, MALDI-TOF-MS, SEM, TEM and TG.

Electrochemical Characterization

A three-electrode electrochemical cell was used to perform the electrochemical characteration of P14AQ. The cell included a platinum counter electrode, a Hg/HgO reference electrode and a working electrode in 13.0 M KOH solution.

The preparation method of the working electrodes for employing cyclic voltammetry and the galvanostatic discharge/charge tests was described as follows. The P14AQ anode was obtained by mixing 60 wt % active material, 30 wt % Ketjen Black (KB) as conductive agent and 10 wt % polytetrafluoroethylene (PTFE 10% w/w H_2O) as binder. For a typical preparation, P14AQ and KB were homogeneously blended using agate mortar and pestle. Then PTFE (10% w/w H_2O) and some drops of ethanol were added into the mixture, and the mixture was rolled into small rounds. Using a tablet press, they were rolled into a 1.2 cm diameter circle stainless-steel gauze (Alfa Aesar, 200 mesh woven from 0.05 mm dia wire, Type 304 Wire Cloth) (**Fig. S1**). Finally, the as-prepared P14AQ anode was dried at 80 °C in vacuum oven. The areal mass loading of P14AQ is about 1-2 mg cm^{-2}. The cathode was removed from commercially available Ni-MH battery (PISEN AA/HR 15/51). To obtain a functional electrode, the PISEN battery was set to discharge with a current of 500 mA until reaching 0.1 V. When this finished, it was again set to discharge with 100 mA until reaching 0.1 V to ensure almost complete discharge. After discharging, the battery was cut open and the $Ni(OH)_2$ sheet was taken out and used directly. The composition and morphology of the $Ni(OH)_2$ sheet are shown in **Fig. S8-S10.** It is assumed that the commercial NiMH battery is packed in a heavy AA casing and it has a capacity of 2500 mAh. The mass of removed cathode is about 12.5 g. Therefore, the material loading is 200 mAh g^{-1}, which fitted well with the land data (**Fig. S11**).

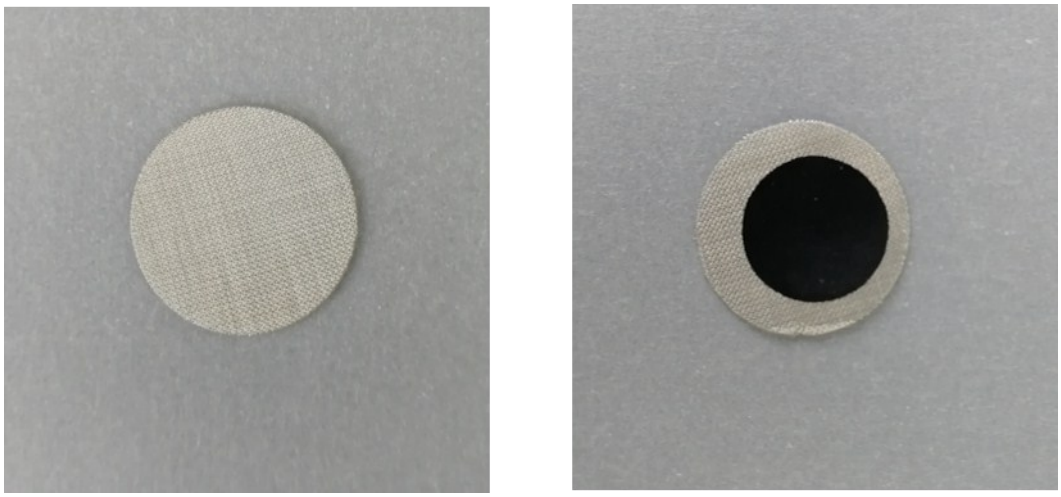

Fig.S1 The stainless-steel gauze, 12 mm in diameter (left) and the as-prepared P14AQ anode (right).

The full cells were assembled in CR2032 cases in which filter paper was used as the separator between cathode and anode. The electrolyte was 13.0 M KOH. The pore of the filter paper was 30 to 50 mm provided by Wohua Filter Paper Limited Company (Hangzhou). The cathode is reused from commercially available NiMH battery (PISEN AA/HR 15/51). The mass ratio of active material of cathode and anode is 1.2:1.

Calculation of energy density of the P14AQ/Co-$Ni(OH)_2$ system.

The system based on Co-$Ni(OH)_2$ cathode and P14AQ anode is a dual-ion battery,and the KOH in the electrolyte is consumed during the charging process ($Ni(OH)_2$ is oxidized to NiOOH). Thus, the active materials of the system should contain both the electrode active materials ($Ni(OH)_2$ + P14AQ) and the consumed KOH. The energy density of P14AQ/Co-$Ni(OH)_2$ system can thus be evaluated according to Equation S1 as follows:

$$E = \frac{Q \times m_{anode} \times V}{m_{anode} + m_{cathode} + m_{KOH}} \quad (S1)$$

where E is the energy density of the electrodes (based on the actice materials mass) and consumed KOH, Q is the discharge capacity based on the anode active material mass (190 mAh g_{anode}^{-1} at 8 C, Figure 2c), V is the average voltage of the rechargeable battery (1.0 V, Figure 2b), m_{anode} is the mass of anode acive material (P14AQ), $m_{cathode}$ is the mass of cathode acive material ($Ni(OH)_2$) and m_{KOH} is the consumed KOH. It should be noted that equal molar KOH is consumed with $Ni(OH)_2$ during the charge process.

Safety Statement

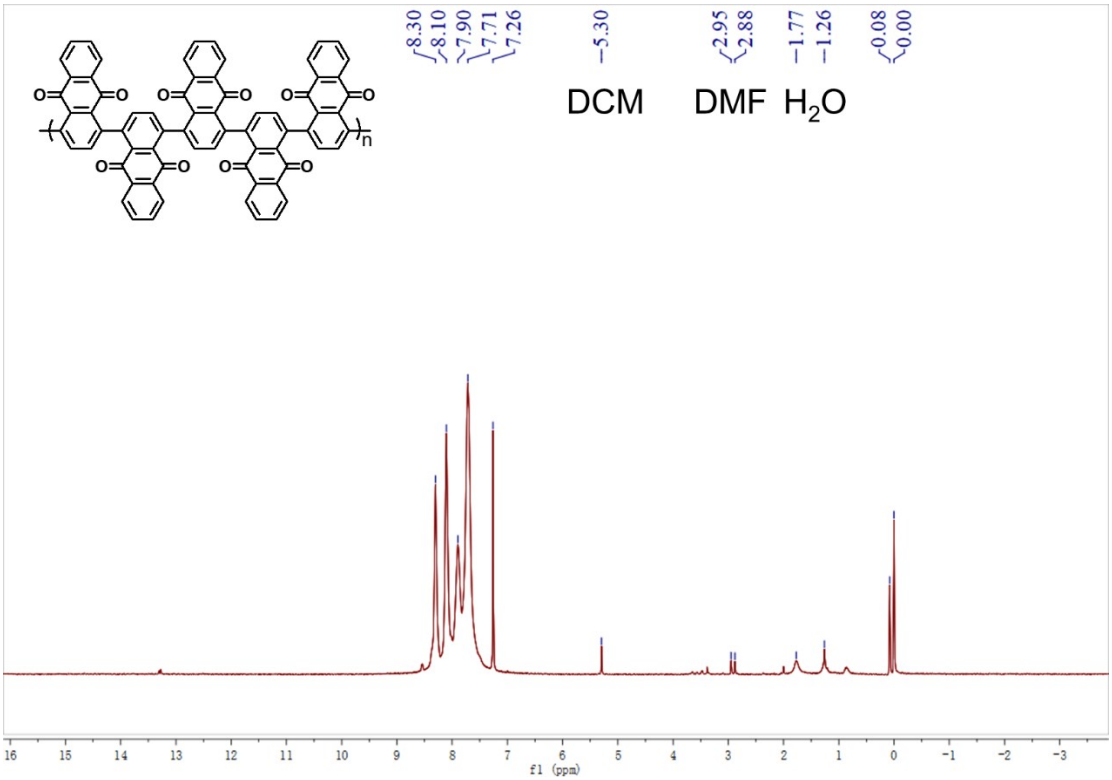

No unexpected or unusually high safety hazards were encountered.

Fig. S2 ^{1}H NMR (400 MHz) of P14AQ in d-chloroform, ^{1}H NMR (400 MHz, $CDCl_3$): δ=7.72, 7.90, 8.10, 8.30 ppm. Total six integrated protons were corresponding to the aromatic hydrogens in each anthraquinonyl moiety. Other peaks should belong to residual solvent: 5.30 ppm (dichloromethane, DCM), 2.95, 2.88 ppm (N,N-Dimethylformamide, DMF), 1.77, 1.26 ppm (water).

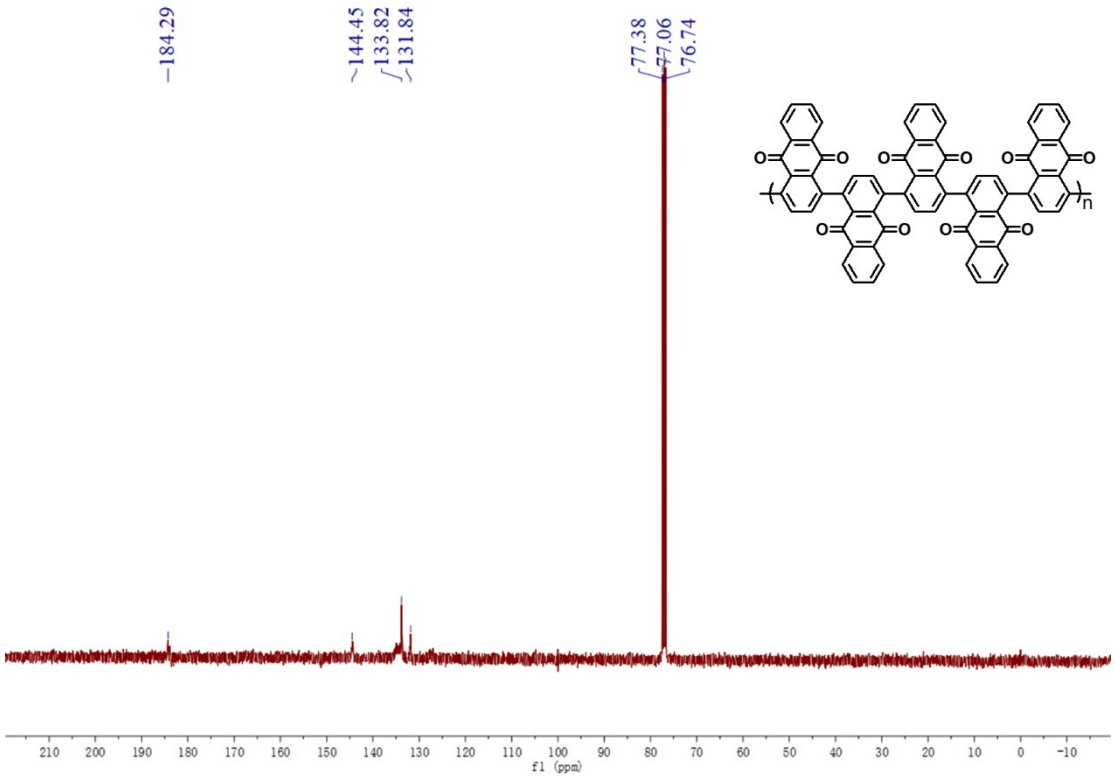

Fig. S3 ^{13}C NMR (400 MHz) of P14AQ in d-chloroform. Some of the broad signals in range of 125-136 ppm prevent the accurate peak selection and interpretation. Multiple signals at 183-185 ppm suggest the presence of the C=O groups in polymer.

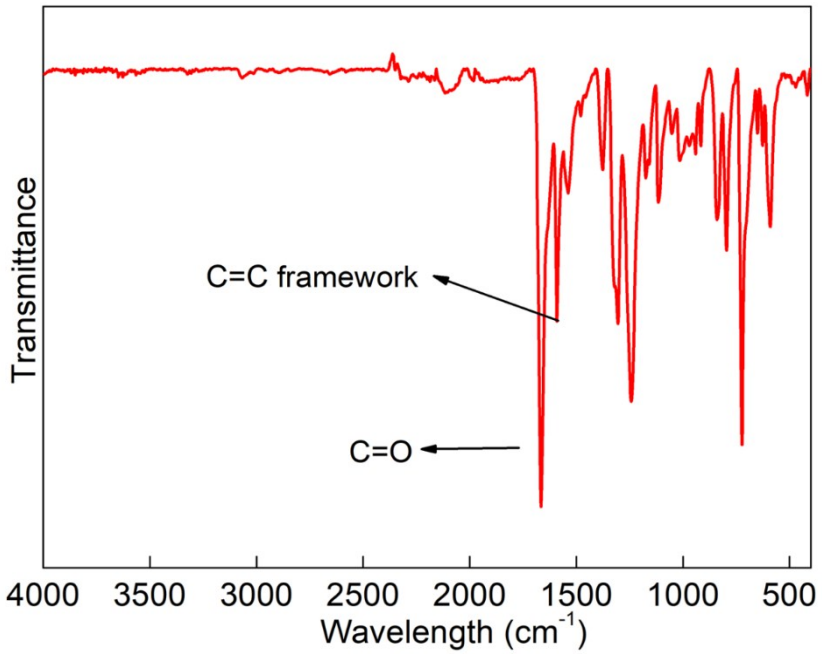

Fig. S4 FT-IR spectroscopy of P14AQ powder. A characteristic signal at 1663 cm^{-1} was observed, corresponding to the typical C=O double bond stretching. Signal at 1592 cm^{-1} belongs to C=C stretching vibration.

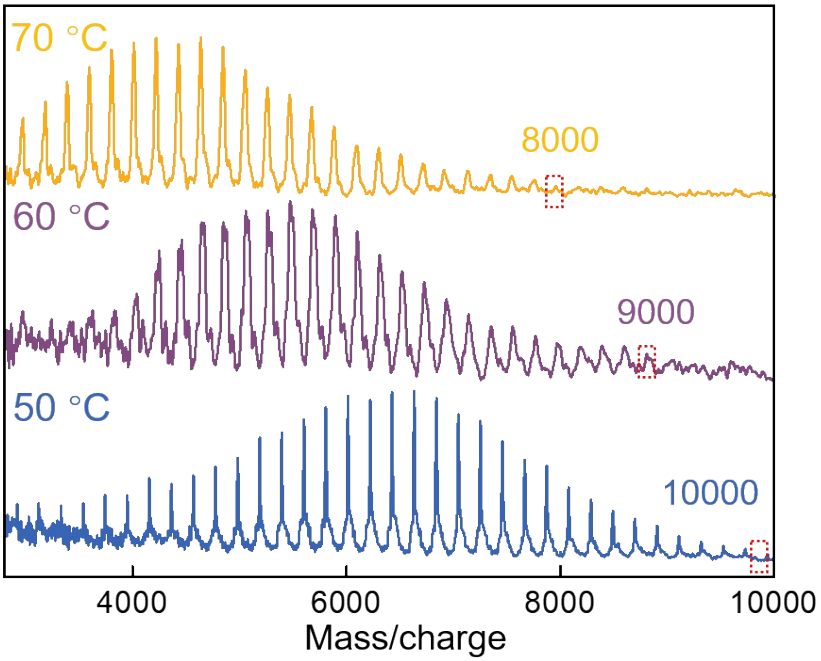

Fig. S5 MALDI-TOF-MS for P14AQ at 50, 60 and 70 °C.

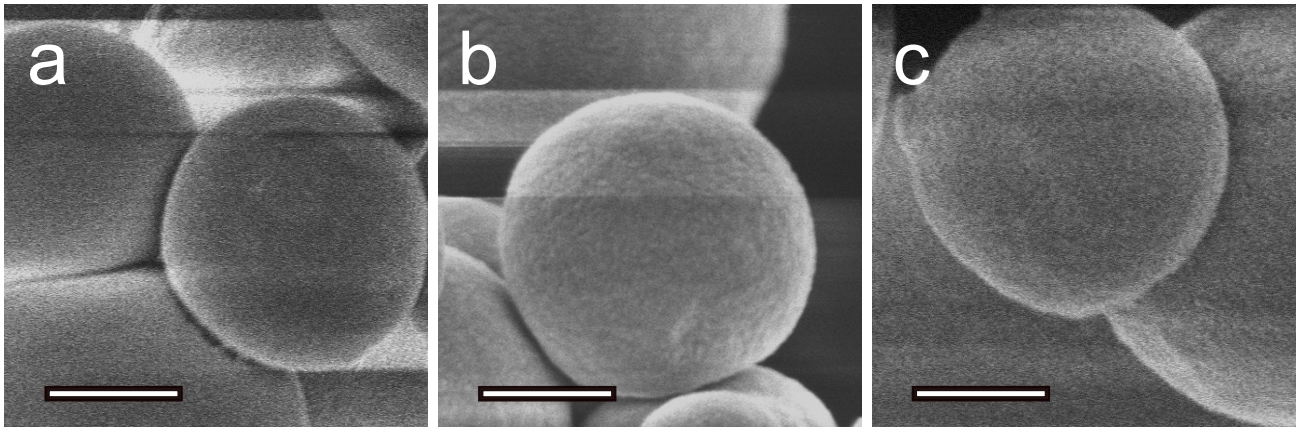

Fig. S6 SEM of P14AQ: (a) M-8000; (b) M-9000; (c) M-10000. Scale bar represents 100 nm.

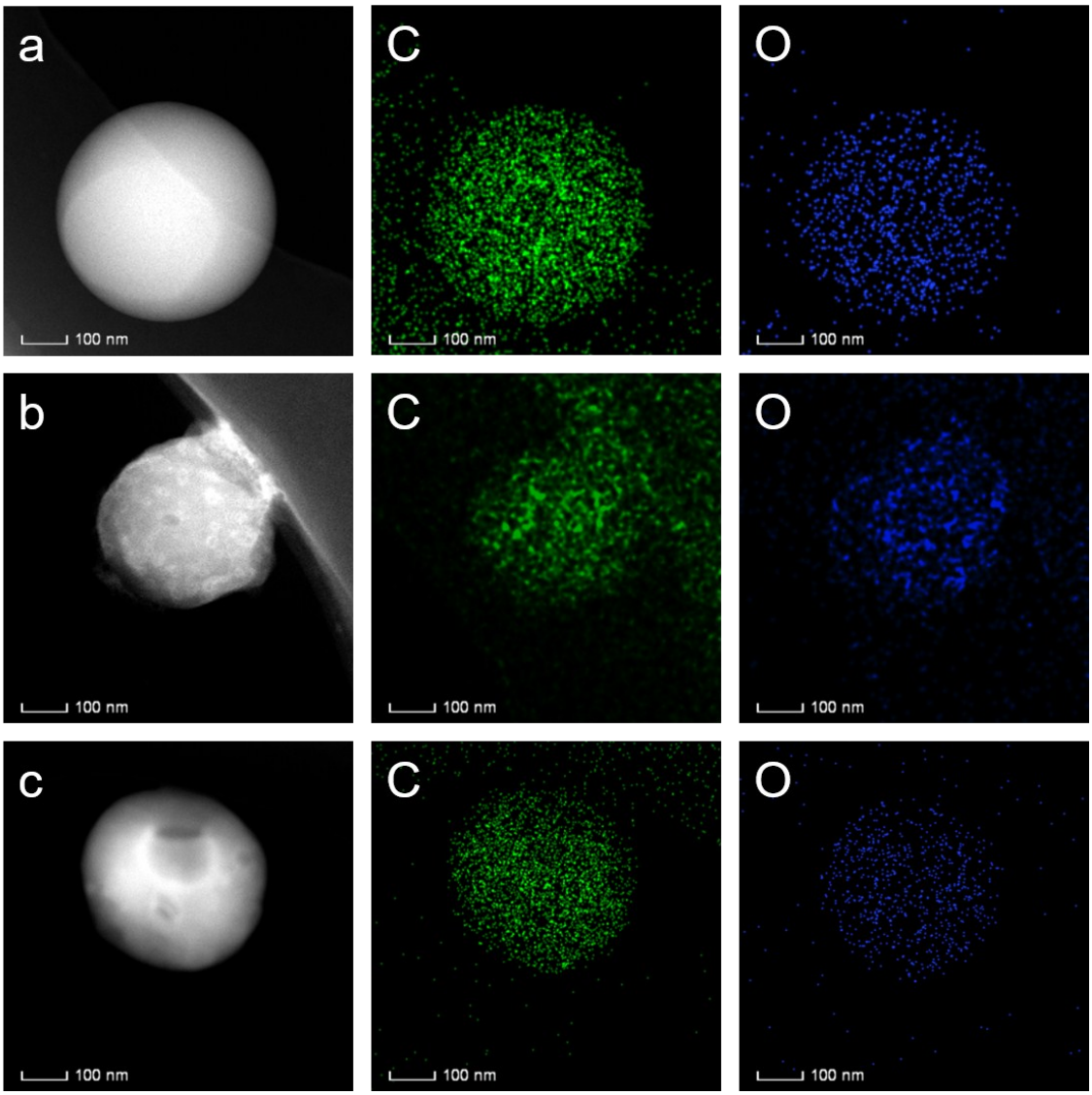

Fig. S7 TEM and EDS-Mapping of P14AQ: (a) M-8000; (b) M-9000; (c) M-10000.

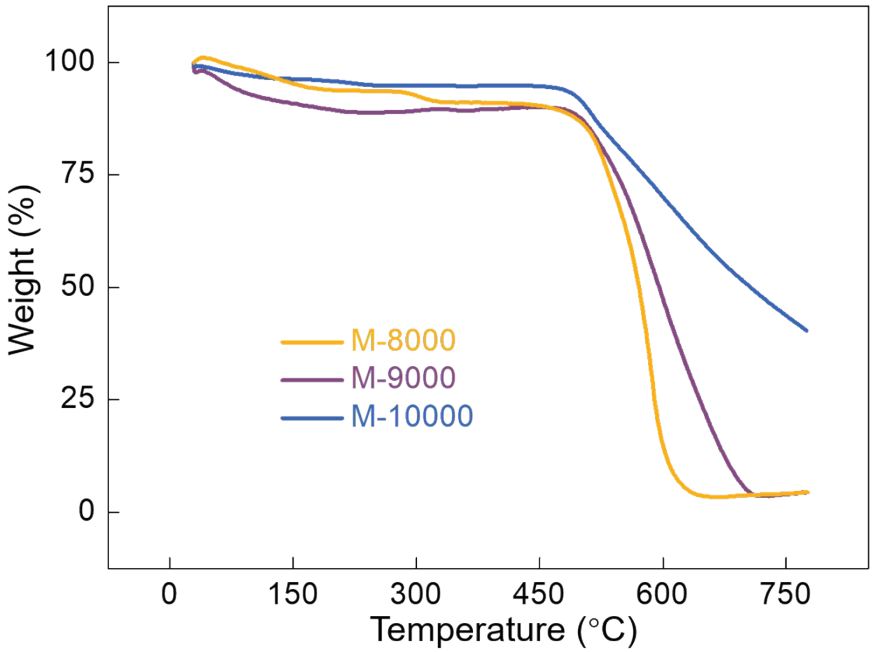

Fig. S8 TG curves of M-8000, M-9000 and M-10000 in ambient air atmospheres at a heating rate of 5 °C min^{-1}.

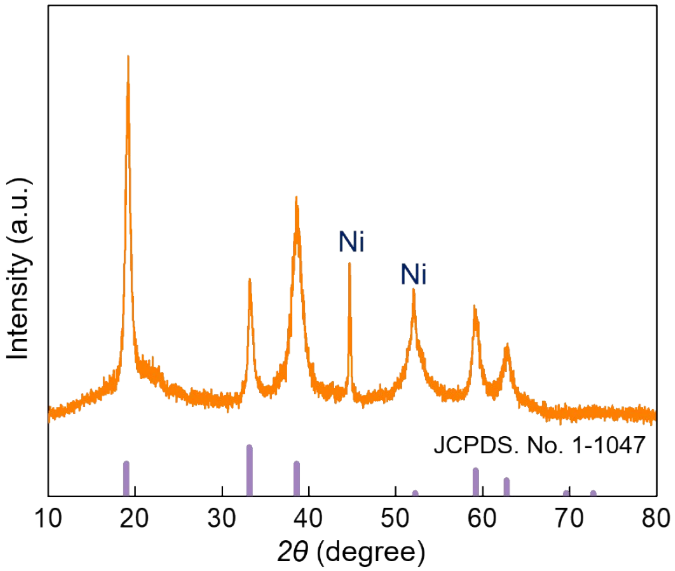

Fig. S9 XRD patterns of reused cathode material from commercially available NiMH battery.

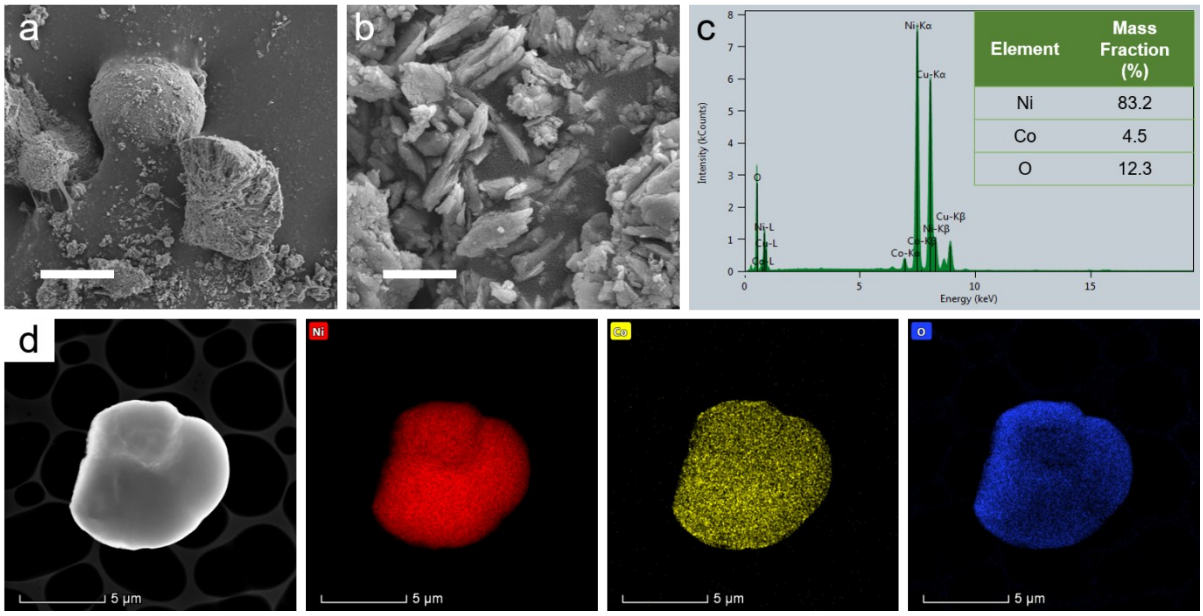

Fig. S10 (a) SEM of cathode. Scale bar represents 5 µm. (b) SEM of cathode. Scale bar represents 500 nm. (c) Mass fraction of the cathode material. (d) TEM and EDS-Mapping of the cathode material.

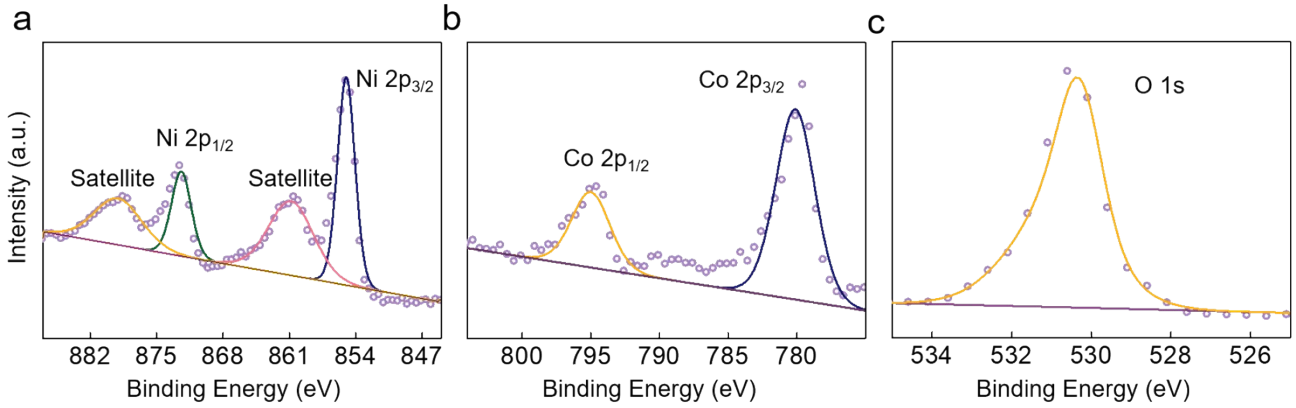

Fig. S11 (a) Ni 2p (b) Co 2p (c) O 1s XPS spectra (X-ray photoelectron spectroscopy) of cathode.

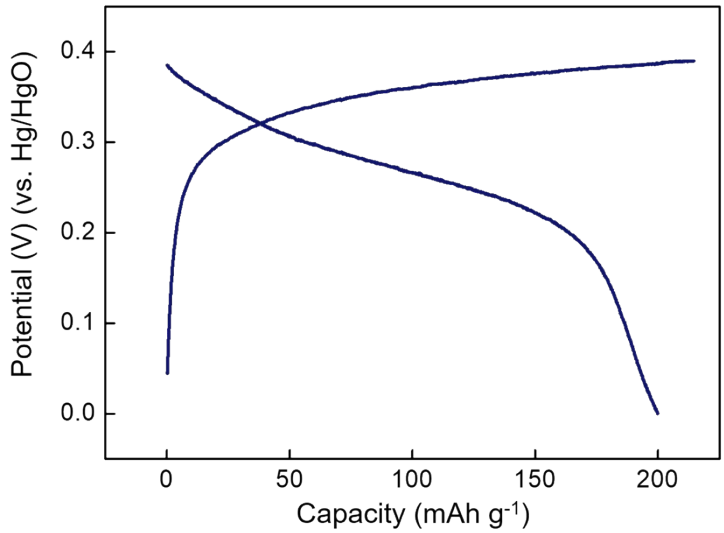

Fig. S12 The galvanostatic profiles of Co-Ni$(OH)_2$ at 260 mAh g^{-1} in 13.0 M KOH.

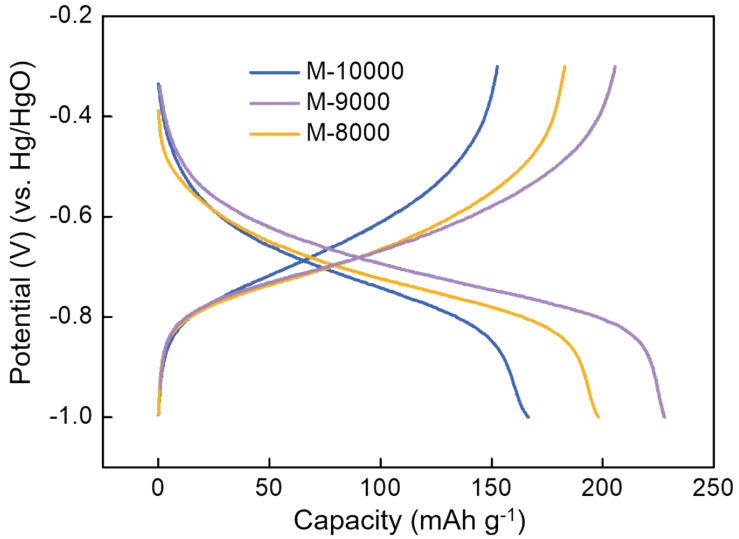

Fig. S13 The galvanostatic profiles of M-8000, M-9000 and M-10000 at 1 C (260 mAh g^{-1}) in 13.0 M KOH.

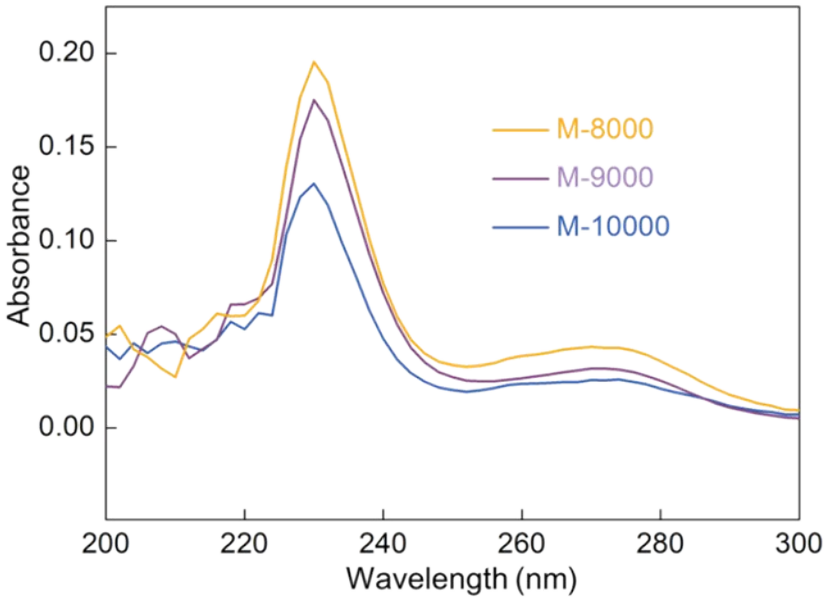

Fig. S14 UV-vis of the separators of M-8000, M-9000 and M-10000 in dichloromethane after charging to 1.2 V for the first time.

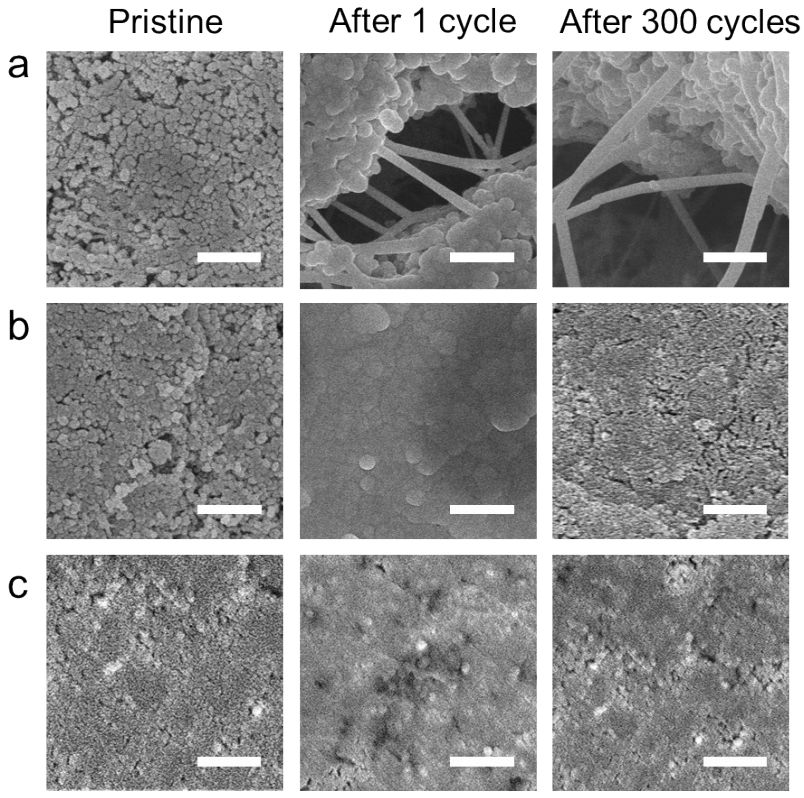

Fig. S15. Comparison of SEM in discharged states for the battery cells of each polymer anode material: (a) M-8000; (b) M-9000; (c) M-10000. Scale bar represents 500 nm.

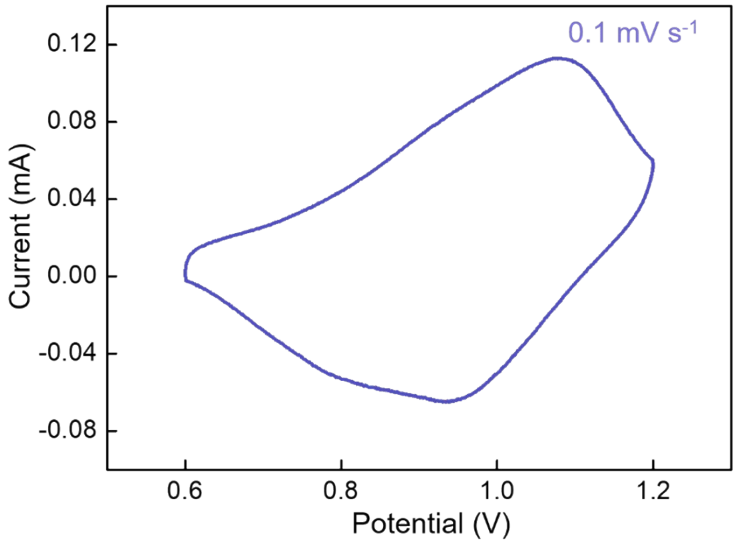

Fig. S16 CV of P14AQ/Co-Ni(OH)$_2$ battery at 0.1 mV s^{-1}.

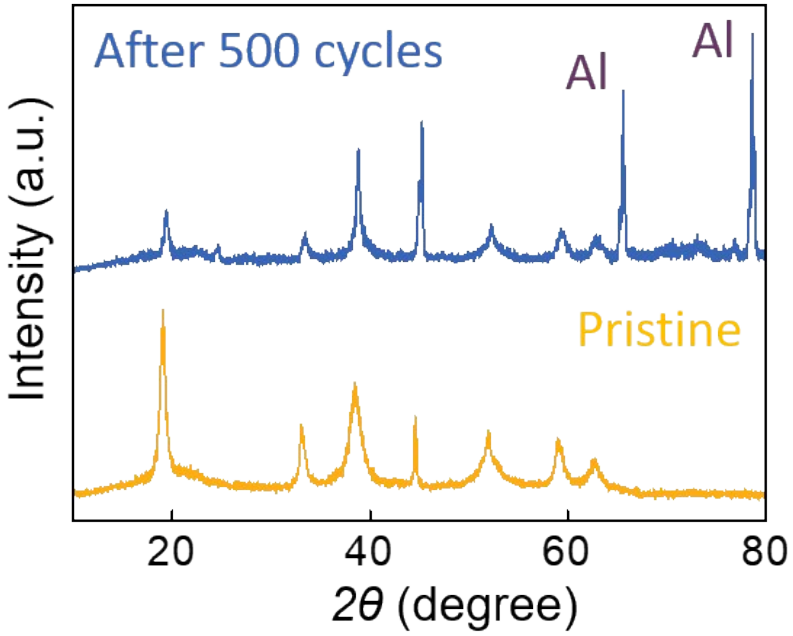

Fig. S17 Comparison of XRD of the cathode material. In order to prevent the effects of air, the disassembly of battery, washing and drying of the electrode were carried out in a glove box. And the electrode sheets were wrapped with aluminum foil during testing.

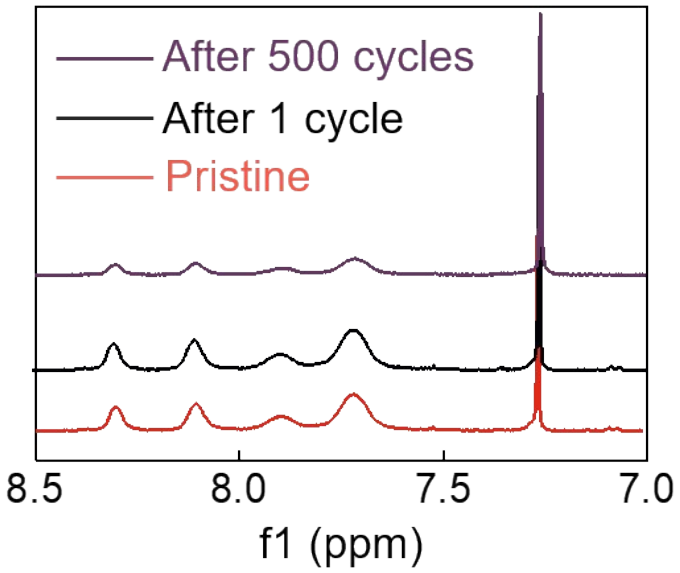

Fig. S18 Comparison of NMR of the M-9000 at pristine, after 1 cycle and after 500 cycles.

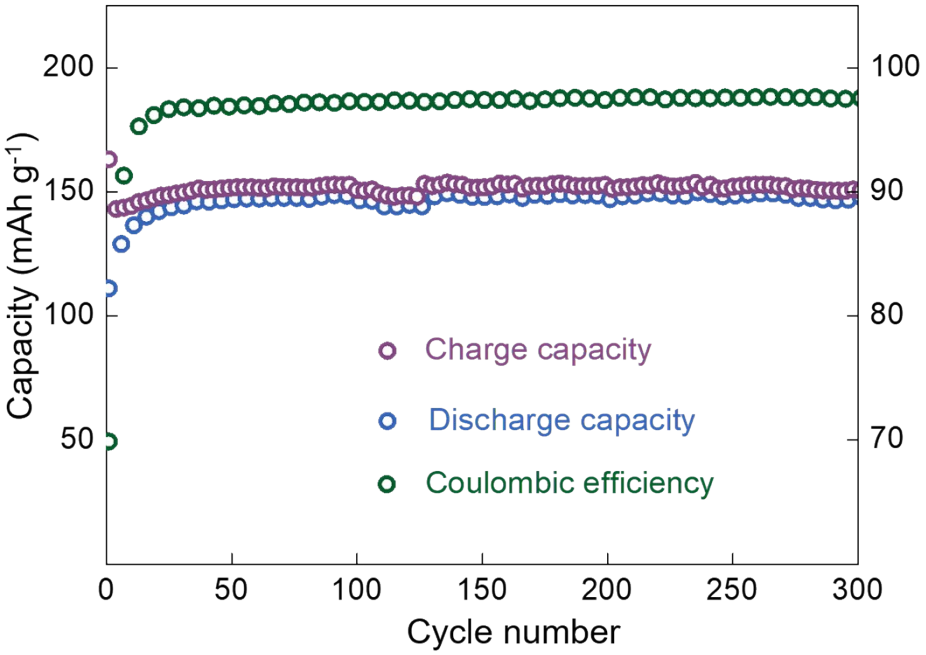

Fig. S19 The cycling performance and Coulombic efficiencies of the given M-9000/Co-Ni(OH)$_2$ battery at 1 C (260 mA g-1) at -30 °C.

Fig. S20 The photograph of 13.0 M KOH at -40 °C for 5 hours.

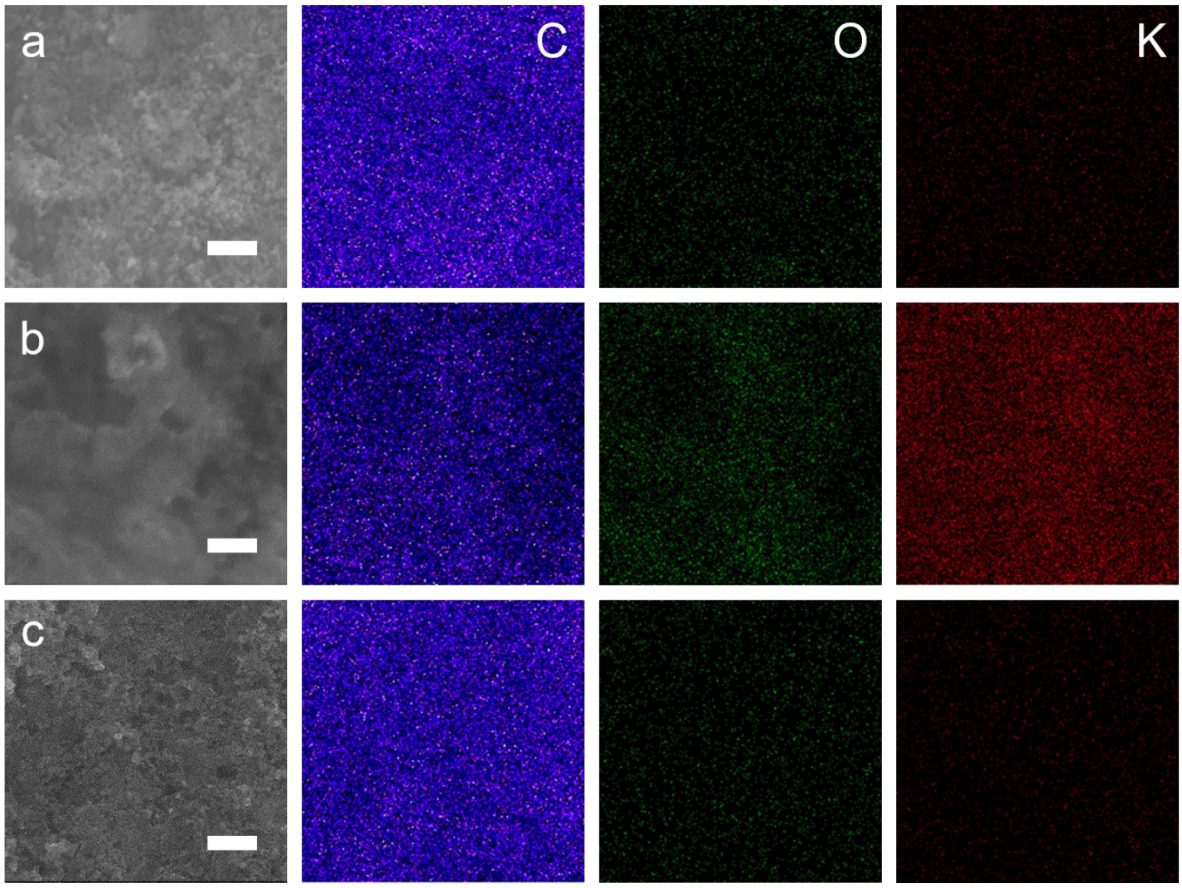

Fig. S21 SEM images and SEM-EDS mappings of C, O, K elemental distributions on P14AQ electrode at (a) pristine, (b) fully charged (1.2 V) state and (c) fully discharged (0.1 V) state. Scale bar represents 500 nm.

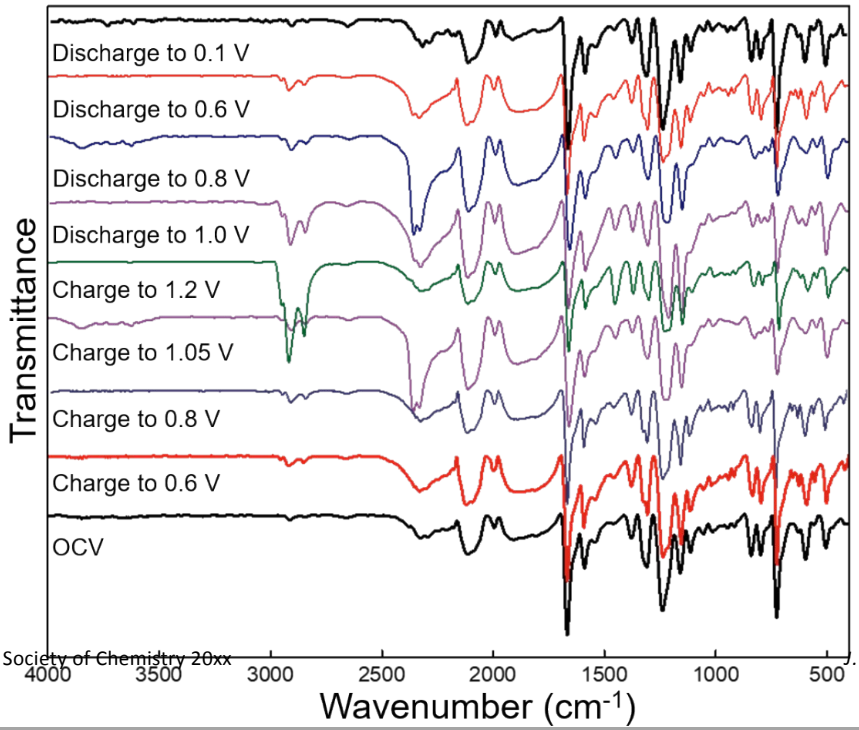

Fig. S22 The full FTIR spectra during the charge/discharge process.

Fig. S23 ^{1}H NMR spectra of P14AQ at pristine, fully charged (1.2 V) state and fully discharged (0.1 V) state in $CDCl_3$.

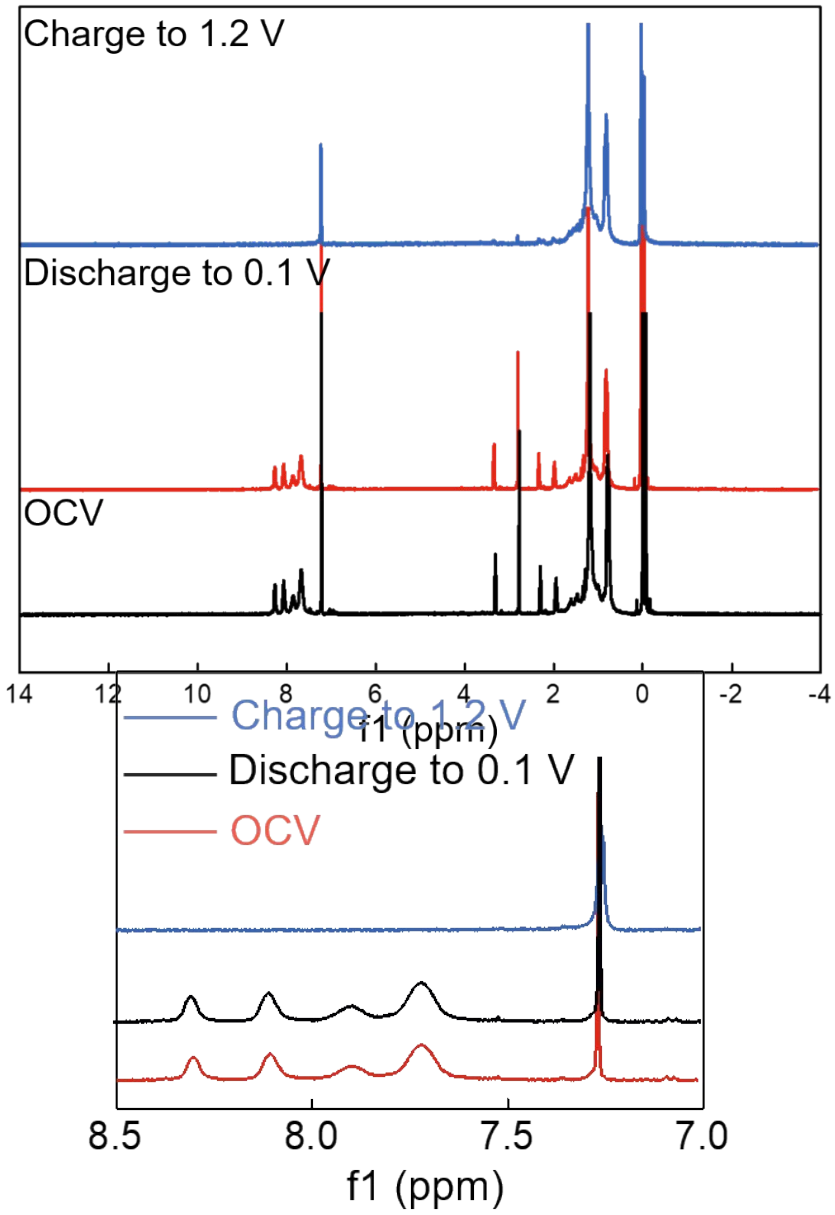

Fig. S24 The full NMR spectra during the charge/discharge process.

Table S1. Comparison of electrochemical characteristics, battery configuration and performance parameters of the different electrode materials for the aqueous potassium-ion batteries.

Entry	Anode	Specific capacity (mAh g^{-1})*	Cathode	Specific energy (Wh kg^{-1})†	Power density (W kg^{-1})	Ref.
1	$K_2FeII[FeII(CN)_6]\cdot 2H_2O$ (PBAs)	120	$K_2FeII[FeII(CN)_6]\cdot 2H_2O$ (PBAs)	65	1250	2
2	polypyrrole (Ppy)	54	$KxCuy[FeIII(CN)_6]$ (CuHCF)	5	100	3
3	3,4,9,10-perylenetetracarboxylic diimide (PTCDI)	125	$K_xFe_yMn_{1-y}[Fe(CN)_6]\cdot zH_2O$ (Mn-rich PBAs)	67	1612	4
4	oligohexane(anthraquinone sulfide) (OHAQS)	75	$Ni(OH)_2$	37	580	5
5	oligo(anthraquinone sulfide) (OAQS)	175	$Ni(OH)_2$	67	1159	5
6	poly(anthraquinone sulfide) (PAQS)	200	$Ni(OH)_2$	83	1159	6
7	DHAQ	223.2	$Ni(OH)_2$	115	133	7
8	OVAQ	228.8	$Ni(OH)_2$	88	102	7
9	OBDTAQ	154.9	$Ni(OH)_2$	77	110	7
10	P14AQ	228	$Ni(OH)_2$	93	1040	this work

* For the anode material. † For a battery consisting of anode/cathode material

1. Z. Song, Y. Qian, M. L. Gordin, D. Tang, T. Xu, M. Otani, H. Zhan, H. Zhou and D. Wang, *Angew Chem. Int. Ed. Engl.*, 2015, **54**, 13947-13951.
2. D. Su, A. McDonagh, S. Z. Qiao and G. Wang, *Adv. Mater.*, 2017, **29**, 1604007.
3. M. Pasta, C. D. Wessells, R. A. Huggins and Y. Cui, *Nat. Commun.*, 2012, **3**, 1149.
4. L. Jiang, Y. Lu, C. Zhao, L. Liu, J. Zhang, Q. Zhang, X. Shen, J. Zhao, X. Yu, H. Li, X. Huang, L. Chen and Y.-S. Hu, *Nat. Energy*, 2019, DOI: 10.1038/s41560-019-0388-0.
5. E. Dražević, A. S. Andersen, K. Wedege, M. L. Henriksen, M. Hinge and A. Bentien, *J. Power Sources*, 2018, **381**, 94-100.
6. Y. Liang, Y. Jing, S. Gheytani, K. Y. Lee, P. Liu, A. Facchetti and Y. Yao, *Nat. Mater.*, 2017, **16**, 841-848.
7. C. Clausen, E. Dražević, A. S. Andersen, M. L. Henriksen, M. Hinge and A. Bentien, *ACS Applied Energy Materials*, 2018, **1**, 243-248.